Design Optimization of a Direct-Drive Wind Generator with a Reluctance Rotor and a Flux Intensifying Stator Using Different PM Types

Ali Mohammadi, *Student Member, IEEE*, Oluwaseun A. Badewa, *Student Member, IEEE*, Yaser Chulaee, *Student Member, IEEE*, Donovin D. Lewis, *Student Member, IEEE*, Somasundaram Essakiappan*, *Senior Member, IEEE*, Madhav Manjrekar*, *Senior Member, IEEE*, and Dan M. Ionel, *Fellow, IEEE*

***Abstract*—This paper presents a large-scale multi-objective design optimization for a direct-drive wind turbine generator concept that is based upon an experimentally validated computational model for a small-scale prototype motor of the same type. By integrating an outer reluctance-type rotor and a segmented stator with toroidally wound single-coil modules containing spoke-type PMs, the design optimization aims to minimize losses, active mass, and torque ripple while adhering to a power factor constraint. The AC windings and PMs are positioned in the stator and this concept enhances flux concentration, enabling the use of more affordable high energy non-rare-earth (special type) magnets. The exterior rotor follows a simplified reluctance-type configuration, eliminating active electromagnetic components. The operational principle, described in detail, guides design studies using electromagnetic 2D finite element analysis (FEA), showcasing the potential of this configuration to match rare-earth PM performance, with special type PMs, thus addressing cost and supply challenges. Furthermore, alternative materials including the substitution of aluminum wire for copper wire, have also been investigated in this study. The proposed multi-objective design optimization uses the response surface method (RSM) to initiate the optimization and the results on a 3MW, 15rpm generator, highlight the benefits of this topology, achieving competitive metrics like goodness, specific thrust, and efficiency without rare-earth permanent magnets.**

***Index Terms*—Direct-drive generator, wind turbine, synchronous machine, flux-switching, flux-reversal, double-salient, design optimization, spoke permanent magnets, toroidal winding, flux-intensifying topology.**

I. Introduction

Wind power is important in reducing greenhouse gas emissions and addressing climate change. The increasing energy demand has driven a shift toward renewable sources, with wind power at the forefront and among the fastest-growing renewable sources. The International Energy Agency foresees that renewable energy will contribute to 30% of global electricity by 2024. The global renewable energy capacity is projected to surge by about 2400 GW (75%) between 2022 and 2027, accompanied by a nearly 50% increase in annual onshore and offshore wind installations by 2027 [1].

In the past decade, the offshore wind generation sector has played an important role in the global wind industry and experienced significant annual expansion, where projections indicate a doubling of its market share by 2025 [2], [3]. As a result of recognizing the energy potential of offshore wind, countries worldwide have been prompted to integrate it into their energy portfolios. This shift is supported by a study reported by Blaabjerg and Ionel, suggesting that widespread installations across the North Sea could fulfill the EU's energy requirements by 2025 [2].

Increased demand for wind energy has led manufacturers to target higher power levels for wind turbine generators. Studies such as the work reported by Polinder *et al.* [4] have shown that in geared generators, a common method of adapting high-power wind turbines to synchronous generators involves gearboxes to adapt slow turbine speeds to synchronous generator speeds. Papatzimos *et al.* [5] had reported that gearboxes have a significantly shorter lifespan compared to that of the turbine generator and require expensive maintenance.

Direct-drive wind turbine generators, which eliminate the need for gearboxes, emerge as a more advantageous solution, not only mitigating the reported shorter lifespan and costly maintenance associated with gearboxes, as highlighted by Papatzimos *et al.* [5], but also enhancing overall reliability and efficiency in wind energy systems.

Comparing offshore and onshore wind turbines reveals distinctive characteristics. Offshore wind turbines boast higher power capacity and a simplified design without the need for a gearbox, leading to reduced maintenance requirements. In contrast, onshore wind turbines present advantages such as lower initial costs and mass, but they come with lower power capacity. Additionally, their complex multi-stage gearbox, which may impact efficiency, necessitates more frequent maintenance.

In this paper, which extends previous work by Mohammadi *et al.* [6], [7]; using special type PM types, the design and optimization for a direct-drive wind generator have been carried out. The machine proposed in this paper is of the synchronous type, and the excitation is provided by a combination of PMs that are placed in the stator and with a single barrier reluctance type rotor, which *together* produce an airgap revolving field with a polarity equal to twice the number of rotor protrusions. The machine includes constructive elements that are similar to those found in machines labeled as double salient, flux reversal, and flux switching.

The structure of this paper is as follows: a literature review

*Dr. Somasundaram Essakiappan and Dr. Madhav Manjrekar were with the QM Power, Inc., Kansas City, MO and are now with University of North Carolina at Charlotte, Charlotte, NC, USA.

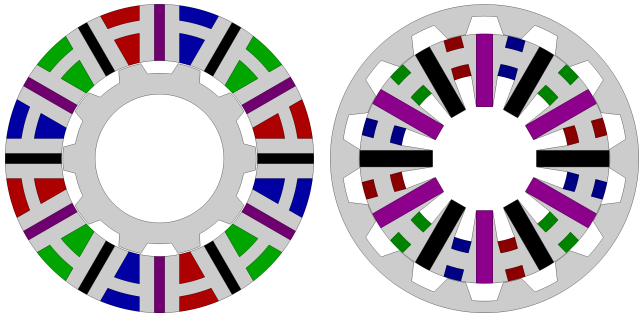

(a) (b)

Fig. 1. Cross-section of the two topologies considered in the study. (a) The reference topology with PMs in the stator with modular configuration and inner reluctance rotor. (b) The topology with the outer rotor and inner stator, benefits from PMs extending into the stator and creating a high flux concentration.

on different aspects of wind turbine generators is provided in Section II. Section III explains the operating principle of the proposed generator. Section IV discusses the optimization of direct-drive generator designs, showcasing the advantages of a flux-intensifying spoke PM stator for higher power density and improved performance. In addition to the cost model, the results and discussions are presented in Section V, demonstrating that the use of special type PMs and aluminum windings can contribute to improved performance and cost reduction in direct-drive wind turbine systems, respectively. Finally, Section VI concludes the paper.

II. Literature Review

Efforts to enhance the performance of wind turbine generators have driven researchers to explore innovative designs, with direct-drive generators gaining popularity. In the design of direct-drive wind generators, the generator inherently has a low speed and is directly connected to the turbine without any intermediate gearbox. This design choice aims to simplify the overall structure, reduce maintenance, and improve efficiency by minimizing energy losses that can occur in traditional gearbox setups. Studies, such as the work by Carroll *et al.* [8], and Tlali *et al.* [9], have demonstrated that direct-drive generators can circumvent the issues associated with gearboxes and improve the wind turbine efficiency.

It has been reported by Gul *et al.* [10], and Zhang *et al.* [11], that direct-drive generators typically have larger dimensions and carry a higher cost and larger mass compared to their geared counterparts, primarily due to the demand for substantial torque at low speeds. The inherent large mass of these turbines has prompted researchers such as Mohammadi *et al.* [7], to investigate the use of aluminum windings as a means to significantly lighten the generator's winding mass without compromising its performance.

Different types and topologies have been proposed for direct-drive applications. Among these, permanent magnet synchronous generators (PMSMGs), have been investigated by researchers such as Semken *et al.* [12], which owing to their improved performance, shows wind turbine manufacturers are increasingly moving toward this type of generator. Wang *et al.* [13], investigated wind generators with self-excited

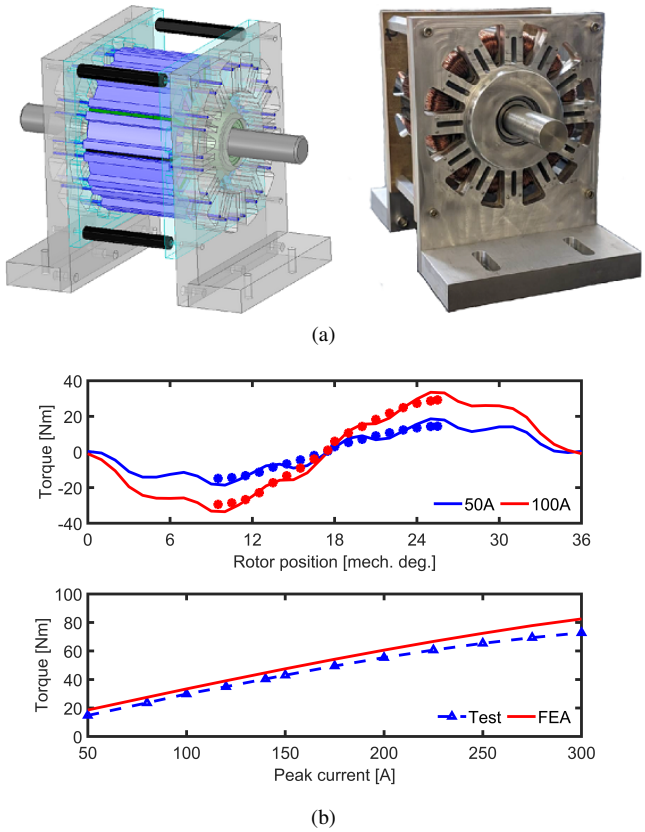

(a)

(b)

Fig. 2. The systematic experimental validation of the computational model on a small-scale prototype motor demonstrates a smaller repetitive structure. (a) The CAD drawing and assembly of the open-frame laboratory prototype motor, and (b) a comparison between the results obtained from FEA and the tests conducted on the prototype.

reluctance topologies, and the vernier-type axial flux design proposed by Mohammadi *et al.* [14], has been considered for direct-drive applications by facilitating increased magnetic flux concentration through the use of high rotor polarities.

Other example studies on wind turbine generators include different topologies for instance in the work of Labuschagne *et al.* [16], on permanent magnet Vernier generator technology, and Tlali *et al.* [9], which compared traditional and conventional PM generators. Husain *et al.* [17], reviewed PM transverse flux machines for direct-drive application, and Chen, *et al.* [18], provided a comparative study for multiple configurations of both radial-flux and axial-flux wind generator topologies.

Boldea *et al.* have conducted multiple studies on high-power, permanent magnet free wind generators. Their investigations encompass designs of various topologies, including direct-drive cage rotor induction generator (CRIG) [19], and direct-drive reluctance synchronous generator (RSG) [20], achieving 10MW of power at 10rpm. Additionally, in another study for PM free generators considering the inclusion of a transmission system, Boldea *et al.* [21], explored an axially laminated anisotropic (ALA) rotor RSG, reporting a power output of 10MW at 480rpm.

Table I
SUMMARY OF MAIN DIMENSIONS AND PERFORMANCE FOR 3MW (NDFEB* AND SPECIAL TYPE PM) DIRECT-DRIVE WIND TURBINE GENERATORS.

Reference	Airgap diameter [m]	Stack length [m]	Efficiency [%]	Specific PM mass [g/Nm]	Specific mass [g/Nm]	Specific thrust [kN/m2]	Goodness [kNm/$\sqrt{W_{loss}}$]
Lehr *et al.* [15]*	5.0	1.9	95.9	1.451	N/A	25.867	5.622
Lehr *et al.* [15]*	5.0	1.9	97.2	1.793	N/A	26.537	6.620
Polinder *et al.* [4]*	4.7	1.2	96.0	0.895	12.684	44.864	5.374
New design A	4.7	1.7	96.9	4.519	33.994	32.180	6.173
New design B	4.8	1.7	96.6	3.027	31.008	31.440	5.902

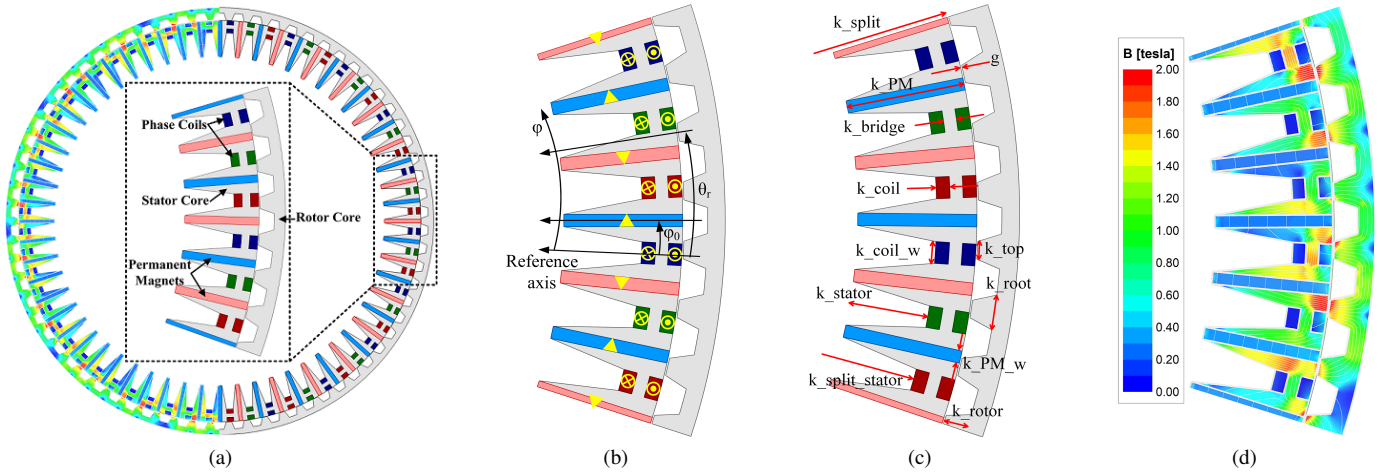

(a) (b) (c) (d)

Fig. 3. (a) The cross-section and enlarged detailed view of the direct-drive generator topology, that produces 1.9MNm torque at 15rpm, (b) the cross-section of the smaller periodicity region for the example generator design with 7 rotor protrusions, (c) geometric design variables used in the parametric model in the multi-objective optimization of the generator under study, and (d) magnetic flux density distribution of the direct-drive wind generator concept.

Many scientific works are progressing toward the elimination of the rare-earth materials from wind generators, for instance, Akuru *et al.* [22], studied the design optimization of a novel rare-earth free flux switching wind generators for small and large power levels. Another example study by Ullah *et al.* [23] was proposed and validated by prototyping a novel dual electrical and dual mechanical wound field flux switching generator, which is brushless, and eliminates the PMs. Ullah *et al.* [24] also proposed a PM-based counter-rotating dual rotor PM flux switching generator for direct drive counter-rotating wind turbine to eliminate slip rings, brushes, and terminate gearbox mechanism.

A design concept, which allows for a high flux concentration ratio by integrating spoke permanent magnets was investigated by Mohammadi *et al.* [6]. This concept not only increases the power density but also improves performance to counterbalance the reduced rotational speeds associated with direct-drive topologies. Additionally, the optimization of the generator's design has the potential to reduce material expenses, particularly by adopting special type PMs. These types of PMs serve as a more cost-effective alternative to the commonly employed rare-earth counterparts in direct-drive wind turbines.

The generator topology was first introduced and validated in a lower pole count reference design, as shown in Figs. 1a, and 2. In the study on the reference design reported by Han *et al.* [25] the core losses were validated at a higher speed, and the copper losses were verified on the prototype shown in Fig. 2, which included a good estimation of end windings used in the prototype.

The reference design was further improved in work done by Badewa *et al.* [26], using an inner stator and outer rotor topology shown in Fig. 1b. In this implementation, the inner stator enables the PMs to extend into the stator and achieve a high flux concentration. The proposed concept explained herein combines the inner stator and outer rotor design with a high polarity which is optimized to use special type PMs such that comparable performance to that with NdFeB PMs is achievable. Furthermore, the dimensions and performance indices of three direct-drive wind generators from literature with rare-earth NdFeB PMs have been summarized in Table I alongside the new designs of this paper.

III. WIND TURBINE GENERATOR TOPOLOGY AND PRINCIPLE OF OPERATION

The configuration of the proposed direct-drive generator uses multiple repetitive modules of the type previously described as shown in Fig. 1, and extended to a higher polarity design for the generator under study as depicted in Fig. 3 to deliver 1.9MNm electromagnetic torque. This topology utilizes stator PMs that separate modules of the core and concentrated AC coils toroidally wound around the back iron, resulting in a high winding factor, as discussed for example in Heins *et al.* [27]. The winding pattern follows the succession of the three phases around the stator circumference. High fault tolerance is achieved by placing only one coil side in each slot.

The stator core has rectangular slots that enable the use of rectangular wire leading to a high slot fill factor and low copper losses. The concentrated coils are toroidally wound

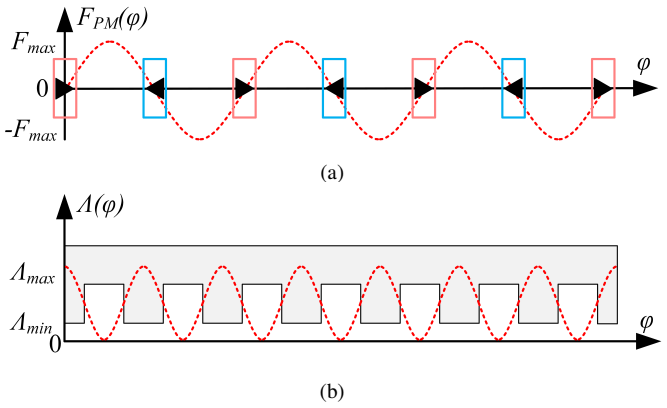

Fig. 4. The MMF-permeance schematic for the proposed generator considering PM only (a), and armature windings with airgap permeance (Λ) (b).

with compact axial ends, providing a further contribution to reducing copper losses. Additionally, the PMs in this topology are placed in the stator, in radial positions, and every two consecutive PMs are magnetized tangentially in opposite directions, which is illustrated in Fig. 4a.

It should be noted that in this design the magnets can substantially extend in the radial direction enabling very high flux concentration and achieving airgap flux densities considerably higher than the remanence of the PM. The winding layout produces an airgap magnetomotive force (MMF) that is similar to that achieved through a fully pitched winding, which is advantageous in ensuring a high fundamental winding factor. Furthermore, depending on the machine's proportions including the number of poles, airgap diameter, and stack length, the end windings facing away from the airgap are relatively short and have a minimal contribution to copper losses.

The reluctance-type rotor does not include any active excitation components and has a laminated steel core with protrusions, the number and dimensions of which are coordinated with the stator characteristics. The rotor and stator use M19 laminated steel, and Fig. 3b depicts the analyzed minimal region of periodicity, which includes seven rotor protrusions. This section was replicated 10 times to create the full generator cross-section, which has 70 rotor protrusions corresponding to 140 magnetic poles.

It is worth mentioning that the flux density distribution in the core at rated load is below 2T as shown in Fig. 3d, therefore saturation is avoided. A detailed analysis of the magnetic flux in open-circuit and under a rated current density of 3A/mm^2 revealed that a flux leakage of approximately 10% has been observed at the inner side of the stator core, which is relatively small considering the overall flux concentration capability of this design.

The open-circuit (OC) PM field and the armature field are analyzed using the MMF-permeance model depicted in Fig. 4 and presented in [6] to describe the working principle of the presented generator concept and the torque generation process. To study the OC PM field, the armature windings are not considered, leaving only the PMs as the source of the magnetic field [25]. Without considering the stator slotting effect, the airgap flux density distribution produced by PMs can be calculated as:

$$\begin{aligned} &B_{PM}(\varphi,t) = \\ &F_{PM}P_{PM}\frac{\Lambda_{avg}}{\kappa_{PM}}\sin\left(\kappa_{PM}\left(\varphi-\varphi_0\right)\right)+ \\ &F_{PM}P_{PM}\frac{\Lambda_{pp}}{4\kappa_{PM}}\sin\left(\kappa_{PM}+N_{pr}\right)\cdot \\ &\left[\varphi-\frac{N_{pr}\omega_r t-\kappa_{PM}\varphi_0-N_{pr}\theta_r}{\kappa_{PM}+N_{pr}}\right]+ \\ &F_{PM}P_{PM}\frac{\Lambda_{avg}}{\kappa_{PM}}\sin\left(\kappa_{PM}-N_{pr}\right)\cdot \\ &\left[\varphi+\frac{N_{pr}\omega_r t+\kappa_{PM}\varphi_0-N_{pr}\theta_r}{\kappa_{PM}-N_{pr}}\right], \end{aligned} \tag{1}$$

where, $B_{PM}(\varphi,t)$ is the flux density distribution in the airgap due to PMs; F_{PM} the amplitude of the square-wave MMF created by PMs; Λ_{avg} the average of the maximum and minimum of the airgap permeance; P_{PM} half of the number of PMs; φ the mechanical angle alongside the peripheral of the airgap with its initial position with respect to the reference axis φ_0; κ_{PM} is equal to $(2k+1)P_{PM}$ and k is a positive integer; N_{pr} the number of rotor protrusions, ω_r the mechanical speed of the rotor, and θ_r and t are the rotor initial position and time, respectively. Considering only the PMs as the source of magnetic flux, according to Eq. (1), there are three groups of flux density harmonics with different rotational speeds and respective pole pairs of κ_{PM}, $\kappa_{PM}+N_{pr}$, and $|\kappa_{PM}-N_{pr}|$.

The distribution of airgap flux density as a result of disregarding the PMs and only considering the armature winding $B_{AR}(\varphi,t)$ [28], can be similarly obtained:

$$\begin{aligned} &B_{AR}(\varphi,t) = \left(\frac{3}{\pi}\right)W_{max}I_m\Lambda_{avg}\cdot \\ &\sum_{m}^{\infty}\left(\frac{P_{AR}}{m}\right)\sin m\left[\varphi-\varphi_{a0}-\left(\frac{\omega t-\varphi_a}{m}\right)\right]+ \\ &\left(\frac{3}{4\pi}\right)W_{max}I_m\Lambda_{pp}\sum_{m}^{\infty}\left(\frac{P_{AR}}{m}\right)\sin\left(m+N_{pr}\right)\cdot \\ &\left[\varphi-\frac{\omega t+\varphi_a-m\varphi_{a0}-\left(N_{pr}\omega_r\right)\left(t+1\right)}{m+N_{pr}}\right]+ \\ &\left(\frac{3}{4\pi}\right)W_{max}I_m\Lambda_{pp}\sum_{m}^{\infty}\left(\frac{P_{AR}}{m}\right)\sin\left(m-N_{pr}\right)\cdot \\ &\left[\varphi-\frac{\omega t+\varphi_a-m\varphi_{a0}+\left(N_{pr}\omega_r\right)\left(t+1\right)}{m-N_{pr}}\right], \end{aligned} \tag{2}$$

where, $B_{AR}(\varphi,t)$ is the distribution of airgap flux density solely from the armature windings; W_{max} and I_m are the sawtooth wave winding function and phase current peak values, respectively; P_{AR} is the number of coils per phase in the armature winding; variables m, r, and t are positive integers, and $m=3r+1=tP_{AR}$; ω is the electrical frequency; φ_a the phase angle relative to φ_{a0} from the reference axis to the winding axis with three groups of flux density harmonics with m, $m+N_{pr}$, and $|m-N_{pr}|$ pole pairs.

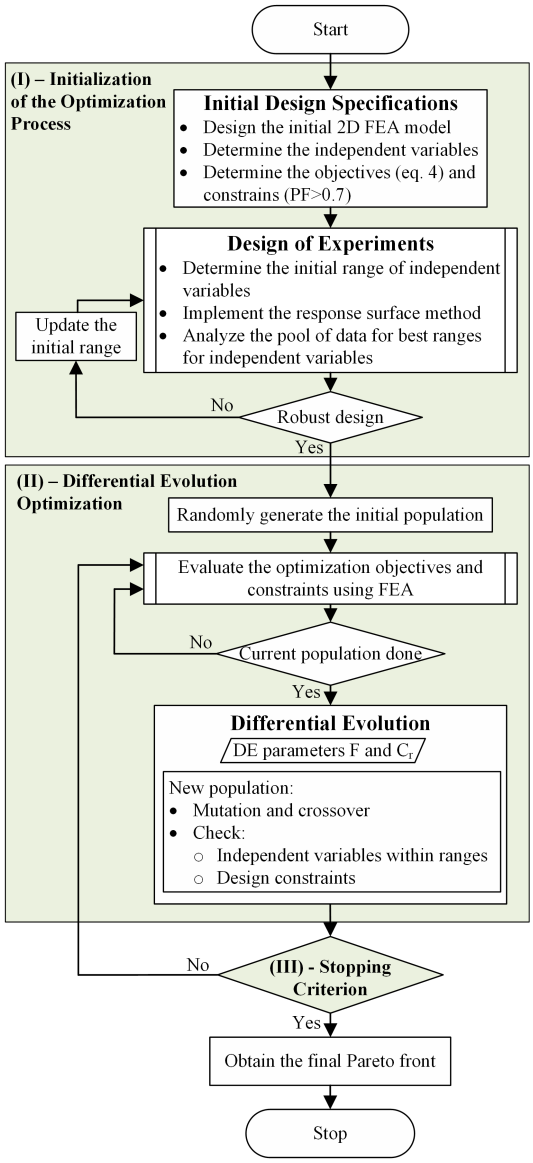

Fig. 5. The proposed two-level optimization algorithm is based on the differential evolution method using the design of experiments for initialization with an interior loop.

The overall electromagnetic performance of the machine is determined by the combination of stator PMs, rotor protrusions, and stator toroidal coil layout. The electromagnetic torque can be obtained using the principle of virtual work with the closed-form analytical airgap flux density distributions of PMs, $B_{PM}(\varphi, t)$, and armature windings, $B_{AR}(\varphi, t)$, and can be expressed by:

$$\begin{aligned} T_{emg} &= \frac{\partial}{\partial \theta_r} \int_V \frac{B(\varphi,t)^2}{2\mu_0} \mathrm{d}V \\ &= \frac{D_s g \ell_{stk}}{4\mu} \frac{\partial}{\partial \theta_r} \int_0^{2\pi} \left[B_{PM}(\varphi,t) + B_{AR}(\varphi,t)\right]^2 \mathrm{d}\varphi, \end{aligned} \tag{3}$$

where, D_s is the stator outer diameter, g the airgap length, and ℓ_{stk} the machine axial stack length. By using the orthogonal properties of sinusoidal behavior, it can be inferred that only the dominant airgap flux density harmonics from the PM and armature fields with pole pairs of 4, 6, 8, 16, 18, and 28 will create a non-zero average electromagnetic torque in the example generator.

Table II
INDEPENDENT VARIABLES FOR THE OPTIMIZATION, THEIR DESCRIPTION BASED ON DESIGN SPECIFICATIONS, AND CORRESPONDING VALUES.

Variable	Description	Min	Max
g	airgap [mm]	5.00	6.00
k_split	split ratio	0.89	0.97
k_PM	PM length ratio	0.82	1.2
k_PM_w	PM width ratio	0.12	0.38
k_bridge	bridge length ratio	0.21	0.44
k_slot	slot length ratio	0.32	0.78
k_slot_w	slot width ratio	0.12	0.38
k_top	rotor pole top ratio	0.24	0.72
k_root	rotor pole root ratio	0.35	0.65
k_rotor	rotor pole depth ratio	0.30	0.70
k_split_stator	stator split ratio	0.93	0.96
k_stator	stator extension ratio	0.78	0.88

The suitable combinations of stator PMs, rotor protrusions, and stator winding patterns that provide non-zero average torque can be derived by analyzing Eq. (3). The designs with 5, and 7 protrusions with a stator including 6 PMs and 6 toroidal coils, and the designs with 10, 14, and seven protrusions with a stator including 12 PMs and 12 toroidal coils, are typical topologies produced by this method. The proposed topology explored herein has 70 rotor protrusions and 60 stator PM and toroidal coils, which are a set of the possible working combinations of rotor protrusions, stator PMs, and coils, which must be multiples of 14 and 12, respectively.

IV. Problem Formulation and Differential Evolution Optimization

The target rated power and speed for the direct-drive wind turbine design under study are 3MW and 15rpm. The literature review along with parametric analysis, revealed appropriate values for the outer diameter, current density, and the number of magnetic poles prior to the optimization while other geometrical variables were systematically adjusted to target the most favorable design. Design optimization techniques are typically employed for seeking optimal designs, with differential evolution (DE) being a popular population-based evolutionary optimization algorithm widely used in various fields.

Differential evolution operates on the principle of improving a group of potential solutions over several iterations [29]. Unlike some other optimization methods, DE does not require any information about the mathematical properties of the problem, making it particularly useful in complex multi-objective optimization scenarios, such as the case under study. Detailed optimization of the proposed design using DE was carried out considering the farthest geometrically and mechanically stable limits that would satisfy the set objective functions.

In wind turbine generators, key objectives include minimal mass and torque ripple and maximal efficiency to ensure cost-effective operation/longevity and structural reliability. Hence,

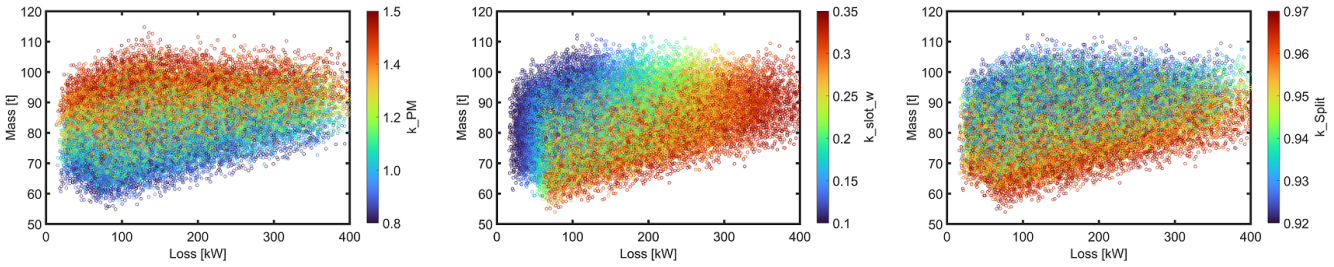

(a) (b) (c)

Fig. 6. The response surface method analysis example results are presented to show the effect of independent variables on the generator's active mass and losses. The independent variables studied are reported in Table II, and example results are shown here for (a) PM depth extension in the radial direction, (b) the coil width in the circumferential direction, and (c) the ratio of airgap diameter to generator outer diameter.

three concurrent optimization objectives in this study are to *minimize* the power loss F_1, active mass F_2, and torque ripple F_3:

$$\begin{aligned} F_1 &= P_\ell = P_{Fe} + P_{Cu}, \\ F_2 &= M_s + M_r, \\ F_3 &= T_r = \frac{T_{\max} - T_{\min}}{T_{avg}} \times 100\%, \end{aligned} \tag{4}$$

with an additional *constraint* only on the power factor (PF) to a minimum value of 0.7. The constraint on PF improves the designs in each generation to have a PF higher than 0.7, which is advantageous in terms of reducing the total power rating of the generator and therefore the inverter cost, which is explained in Section V.

The objective function for power loss was calculated as the sum of the variable and constant losses of the generator, where P_{Fe} represents the core loss (constant losses) and P_{Cu} represents the copper loss (variable losses). The objective function for mass only considers the mass of active components including the stator mass, M_s, combining the mass of the core, winding, and permanent magnets, and the rotor core mass, M_r. The torque ripple is calculated by dividing the difference of the maximum of the electromagnetic torque T_{max}, and minimum T_{min}, by the average T_{avg}.

In this paper, 12 geometrical variables were considered for optimization, as illustrated in Fig. 3c and detailed in Table II. The table provides descriptions and the selected range for each variable. Notably, only the air gap is expressed in absolute values measured in millimeters ("mm").

The upper and lower limits of the design variables were set through an efficient and automated response surface method (RSM) to ensure a robust FEA model and a wide optimization area. The response surface method is a statistical approach used to create models that showcase the relationship between design variables and responses, based on real experiments or simulations. Normalized non-linear regression coefficients provided by RSM show the influence of independent variables on performance indices such as electromagnetic torque.

It should be noted that the RSM implemented in this research follows the typical approach, which is a useful tool to potentially minimize the number of variables and hence the computational effort. In the case of the proposed generator, the operation of which is affected by the non-linearity, it has been observed that all of the variables are substantial.

To manage the complexity of the response function, in this paper a second-order polynomial model was used for RSM assuming a functional relationship with scaled and centered design units. At this step, FEA was employed to generate the initial responses for RSM, focusing on the generator characteristics and performance including mass, torque, and losses, which are influenced by independent design variables.

The FEA results are initially provided to the RSM analysis to generate a range of designs without conducting any extra FEA analysis, as illustrated in Fig. 6. The number of FEA results given to RSM is one order of magnitude smaller than the generated results produced by RSM, which shows the efficiency of this method. These designs have been analyzed to identify the most effective parameters, prevent geometric errors during the optimization process, and establish suitable ranges for the independent variables employed in the optimization, as detailed in Table II.

In order to decide the suitable ranges for the independent variables, for instance, the outcomes of RSM, exemplified in Fig. 6a, aid in defining the ranges for the ratio of PM depth extension in the radial direction to stator depth. To attain the objectives of minimized mass, and losses, it is advisable to focus on the lower end of the specified ranges within the optimization problem. A similar analysis has been performed for the example results shown in Figs. 6b, 6c, and all the independent variables in this study.

The optimization process is depicted as a flowchart in Fig. 5. It should be noted that through the use of a two-pass study, it was made certain that each design was capable of producing the rated torque at the rated speed. In the first step of the process, a predetermined stack length was used to examine the design. The stack length was scaled based on the difference between the simulated torque results and the rated torque and the design was re-evaluated to ensure the target torque was obtained.

Multi-objective optimizations use termination criteria to determine when to stop the process. A hybrid stopping criterion was used in this paper that considered the convergence of the optimization algorithm where the termination criterion was either a maximum number of generations or a minimal improvement in three representative points of the Pareto front for a few consecutive generations [30].

Table III

PERFORMANCE OF THE OPTIMAL DESIGNS ON THE PARETO. THE BEST DESIGNS WITH SPECIAL TYPE PMS SHOW COMPARATIVE PERFORMANCE TO THOSE WITH RARE-EARTH PMS. THE GENERATOR RATED POWER AND SPEED ARE 3 MW, AND 15 RPM, RESPECTIVELY.

Design ID	Outer diameter [m]	Airgap diameter [m]	Stack length [m]	Electromagnetic efficiency [%]	Power factor [–]	Torque density [Nm/L]	Specific thrust [kN/m^2]	Goodness [kNm/$\sqrt{W_{loss}}$]
Best designs with **special type** permanent magnets (B_r = 1T)								
A	5.0	4.7	1.7	96.9	0.76	52.5	32.180	6.173
B	5.0	4.8	1.7	96.6	0.67	52.0	31.440	5.902
Best designs with **rare-earth** permanent magnets (B_r = 1.3T)								
C	5.0	4.7	2.1	97.1	0.90	43.8	34.857	6.380
D	5.0	4.7	2.0	97.2	0.90	45.2	36.432	6.473

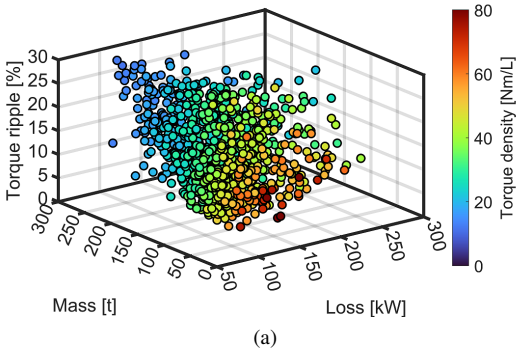

(a)

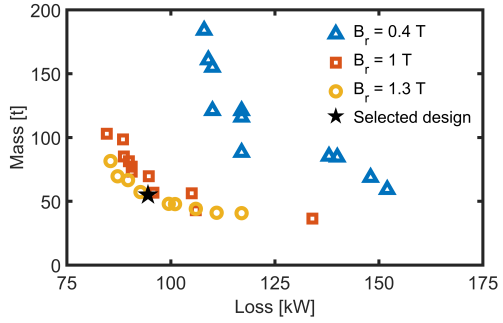

(b)

Fig. 7. The multi-objective optimization results: (a) The results for PM with B_r equal to 1T, showing the torque density of each design as the color map, (b) Pareto optimal designs of optimization results of PMs with different remanent flux densities.

V. OPTIMIZATION RESULTS, DESIGN VARIATIONS, AND DISCUSSION

Multiple designs were optimized exploring a range of permanent magnet materials, each with a unique remanent flux density (B_r). To this end, ferrite and special type PMs with B_r values of 0.4 and 1T, as well as rare-earth magnetic materials with B_r of 1.3T were examined. A population size of fifty different designs per generation was used in each scenario to ensure an extensive exploration of the design space. The outcomes of the optimization process for each condition are depicted in Figs. 7 and 8. To evaluate the performance of the generated designs, 2D-FEA simulations were conducted using Ansys Electronics Desktop 2023 software [31].

A. Optimization Results

The optimization results for non-rare-earth permanent magnet materials with a remanent magnetic flux density of 0.4T, shown in Fig. 8a, indicate that the optimal designs with low torque ripple, minimum losses, and high power factors, tend to have higher masses. The torque ripple of the selected designs is shown as the size of each point in data presented in Fig. 8, which has a minimal effect on the performance due to the very high mass and inertia of the active components.

The power factor is high for the majority of designs, and in some is close to unity, which contributes to a smaller power electronic unit. Also, for design targets of minimum mass, losses, and torque ripple with rare-earth permanent magnets, with optimization results shown in Fig. 7a, the best designs have high torque density which is in line with expectations.

The Pareto fronts of the optimal designs of the three PM materials used for the wind generator under study are combined and depicted in Fig. 7b. The results show that the Pareto fronts of the optimal designs using permanent magnets with a remanent flux density of 0.4T are clearly distinguished from generators that use PMs with a B_r of 1 and 1.3T.

Optimization results indicate that by utilizing high-energy special type PMs produced by the company Niron Magnetics [32], it is possible to achieve comparable performance to direct-drive generators that employ rare-earth PMs, as investigated in the literature reported in Table I. It is also shown that the selected designs have a higher PM mass compared to designs in the literature and therefore have a higher specific PM mass. Compared to NdFeB, the special type permanent magnets introduced by Niron Magnetics have been characterized as having a comparable performance, lower cost, and high price stability [32].

Owing to the high flux concentrating topology, most utilization of permanent magnet flux can be achieved. The flux lines and flux density distribution of the proposed generator are shown in Fig. 3d, where the flux linkage is shown in the airgap. The inner side of the stator can extend and allow for a larger permanent magnet without any significant magnetic flux leakage due to the high reluctance of the magnetic circuit. The significant improvement by the flux-intensifying topology described in this study results in a similar performance to designs with NdFeB while utilizing significantly less expensive permanent magnet materials.

B. Design Variations and Cost Model

The ability of the proposed topology to make use of special type PMs can significantly reduce the cost of permanent magnet materials for this application, which requires a significant amount of PMs. According to the cost model examples

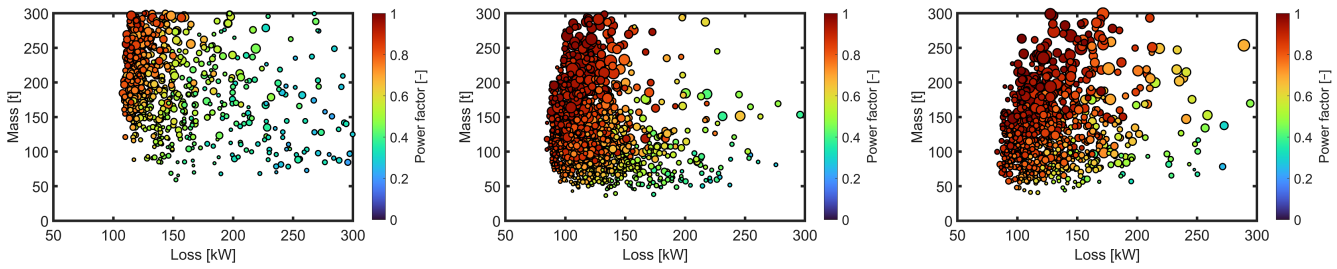

Fig. 8. The multi-objective optimization results, showing the design distribution considering the mass, losses, power factor, and torque ripple for the generators using, (a) B_r= 0.4T, (b) B_r=1T, and (c) B_r= 1.3T. The size of the circle marker for each design is proportional to the torque ripple.

presented by Rosu *et al.* [30], the cost of active materials for machines with ferrite (C_1), special type PMs (C_2), and NdFeB (C_3), relative to per unit mass of laminated steel can be estimated by:

$$\begin{aligned} C_1 &= 5m_{PM} + 8m_{Cu} + 1m_{Fe}, \\ C_2 &= 50m_{PM} + 8m_{Cu} + 1m_{Fe}, \\ C_3 &= 65m_{PM} + 8m_{Cu} + 1m_{Fe}, \end{aligned} \tag{5}$$

where m_{Fe} is the mass of laminated steel, m_{Cu} mass of copper, and m_{pm} mass of permanent magnets.

Example designs marked with a star on the Pareto are shown in Fig. 7b. The optimum design A with special type PMs for example has a goodness of 6.173kNm/$\sqrt{W_{loss}}$, and a specific thrust of 32.180kN/m^2, which are comparable to the designs reported in the literature documented in Table I, that use expensive and high remanence PMs. Four of the best optimization selected designs employing PMs with 1 and 1.3T remanence are depicted in Fig. 9. The designs with special type PMs have a shorter stack length and therefore lower PM mass compared to designs with rare-earth PMs, and hence according to the cost model, the designs with special type PM, have a lower p.u. PM cost. It can be concluded that the cost of active materials for designs with special type permanent magnets is lower than the designs using NdFeB.

The cost of the wind turbine energy conversion system is determined by both the generator and its associated power electronics. The cost of power electronics varies in a wide range with an example reported by the National Renewable Energy Laboratory (NREL), which indicates it does not exceed more than 25% of the total system cost [33]. This cost is influenced by the power rating, with a small allowance for power factor variations. In this research, a constraint was set, requiring a power factor higher than 0.7, which reduces the total power rating of the generator and hence the cost of converters and related components. The implementation of multi-phase windings can further reduce the converter DC link capacitor size and price.

A comprehensive comparison of the geometric and performance indices of the best designs on the Pareto is provided in Table III. The table indicates that achieving comparable performance between special type permanent magnets and their rare-earth counterparts is feasible. The generator novel flux intensifying topology and the applied constraint on power factor have resulted in a longer stack length in designs with rare earth PMs, hence the overall envelope of those designs is larger and results in a lower torque density.

C. Discussion

Short-circuit currents were injected with values of 1p.u. and 2p.u., representing the largest fault condition to investigate demagnetization avoidance in the selected designs. Designs featuring special type PMs and rare-earth permanent magnets, known for their high coercivity, underwent a thorough examination for demagnetization under the mentioned short-circuit currents. In both scenarios, the observed minimum operating point of the PMs was greater than the demagnetization threshold and therefore indicated the absence of demagnetization.

The generator's rated speed is 15rpm which results in a minimal core-to-total loss ratio, with copper losses emerging as the primary factor influencing its efficiency. Additionally, it should be noted in this generator the conductor eddy current losses are negligible and can be further reduced, as suggested in a study by Taran *et al.* [34], through measures such as avoiding filling the top of the slot or increasing the distance of the entire slot from the air gap.

The substitution of copper with aluminum in the armature windings of wind turbines can significantly reduce costs and mass. It should be noted that the mass density between copper and aluminum is significant, where aluminum has a density that is approximately one-third of copper. Furthermore, the cost of aluminum is almost half of copper. Therefore, replacing copper with aluminum can result in a significant reduction in the mass of the wind turbine generator, which can lead to a reduction in the cost of materials and potentially lower the cost of power generated by the turbine.

To investigate the effect of aluminum windings on the performance of wind turbines, as a first attempt pending further optimization work, the optimized configuration using copper windings was adapted to use aluminum. The optimized design topology was modified by replacing the copper windings with aluminum. To ensure that the substitution of materials did not compromise the performance of the wind turbine generator, the selected design was carefully modified to maintain the 3MW power.

Aluminum has lower electrical conductivity compared to copper, which may lead to higher joule losses and reduced

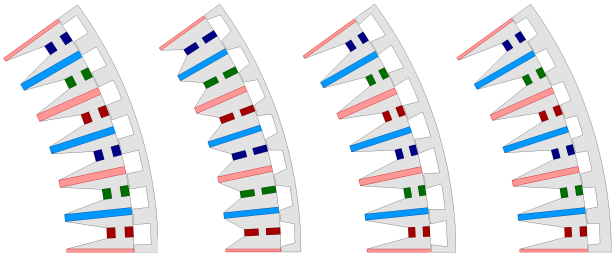

(a) (b) (c) (d)

Fig. 9. Cross-section of the optimized design topologies: (a) and (b) use special type PMs, (c) and (d) use rare earth PMs. Larger copper area in the special type topologies shows the compensation for the PM type.

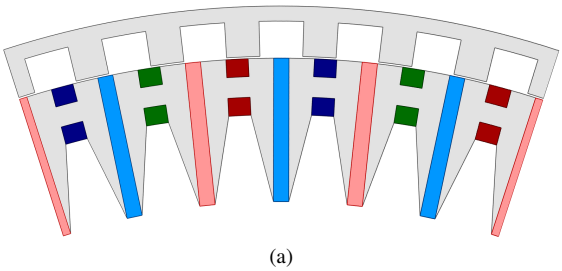

(a)

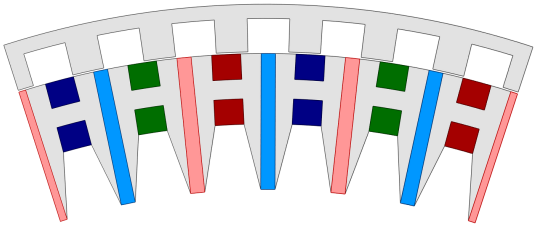

(b)

Fig. 10. Cross-section of the optimized design "A" topology using special type PM with, (a) copper winding, and (b) aluminum winding.

efficiency, therefore to compensate for the difference in conductivity between copper and aluminum, the coil slot area was almost doubled, as shown in Fig. 10. This modification ensured that the aluminum windings could provide similar electrical performance to the original copper windings. In the design with aluminum winding, increased slot size and a smaller yoke, with deeper and narrower teeth, reduces the stator core mass by 2%, contributing to a 2% generator and 36% armature winding mass reduction, which significantly lowers the active material cost.

VI. Conclusion

In this paper, the optimization process yielded direct-drive wind turbine generators featuring different PM types, demonstrating comparable performance in terms of specific thrust, Goodness, and efficiency with low torque ripple and high power factor to that of designs with rare-earth PMs. The proposed design incorporated a robust outer rotor configuration, enhancing magnetic flux through a modular stator with special toroidal windings and spoke PMs. This concept emerged from a validated computational model of a small-scale prototype motor, systematically verified through experiments.

Additional studies confirmed the demagnetization avoidance of the proposed designs. A significant mass reduction by using aluminum winding, exceeding 35% compared to copper winding, was observed. These findings imply potential enhancements in the efficiency, cost-effectiveness, and material utilization of the proposed wind turbine generator.

Acknowledgment

The authors are most grateful to Professor J. F. Eastham of the University of Bath, England, for review, and feedback. This paper is based upon research sponsored by the QM Power, Inc. The support of ANSYS Inc., and University of Kentucky the L. Stanley Pigman Chair in Power endowment is also gratefully acknowledged.

References

[1] International Energy Agency, *Renewables 2022: Analysis and forecast to 2027*. Paris, France: OECD/IEA, 2022, accessed February 2023. [Online]. Available: https://www.iea.org/reports/renewables-2022

[2] F. Blaabjerg and D. M. Ionel, *"Renewable Energy Devices and Systems with Simulations in MATLAB® and ANSYS®"*. CRC Press, 2017.

[3] "Global offshore wind report 2020," *GWEC: Brussels, Belgium*, vol. 19, pp. 10–12, 2020.

[4] H. Polinder, F. F. Van der Pijl, G.-J. De Vilder, and P. J. Tavner, "Comparison of direct-drive and geared generator concepts for wind turbines," *IEEE Transactions on Energy Conversion*, vol. 21, no. 3, pp. 725–733, 2006.

[5] A. K. Papatzimos, T. Dawood, and P. R. Thies, "Data insights from an offshore wind turbine gearbox replacement," *Journal of Physics: Conference Series*, vol. 1104, no. 1, 2018.

[6] A. Mohammadi, O. A. Badewa, Y. Chulaee, D. M. Ionel, S. Essakiappan, and M. Manjrekar, "Direct-Drive Wind Generator Concept with Non-Rare-Earth PM Flux Intensifying Stator and Reluctance Outer Rotor," in *2022 11th International Conference on Renewable Energy Research and Application (ICRERA)*. IEEE, 2022, pp. 582–587.

[7] ——, "Design Optimization of a Direct-drive Wind Generator with Non-rare-earth PM Flux Intensifying Stator and Reluctance Rotor," in *2023 IEEE International Electric Machines & Drives Conference (IEMDC), San Francisco, CA*. IEEE, 2023, pp. 1–6.

[8] J. Carroll, A. McDonald, and D. McMillan, "Failure rate, repair time and unscheduled O&M cost analysis of offshore wind turbines," *Wind Energy*, vol. 19, no. 6, pp. 1107–1119, 2016.

[9] P. M. Tlali, R.-J. Wang, S. Gerber, C. D. Botha, and M. J. Kamper, "Design and Performance Comparison of Vernier and Conventional PM Synchronous Wind Generators," *IEEE Transactions on Industry Applications*, vol. 56, no. 3, pp. 2570–2579, 2020.

[10] W. Gul, Q. Gao, and W. Lenwari, "Optimal Design of a 5-MW Double-Stator Single-Rotor PMSG for Offshore Direct Drive Wind Turbines," *IEEE Transactions on Industry Applications*, vol. 56, no. 1, pp. 216–225, 2020.

[11] Z. Zhang, A. Chen, A. Matveev, R. Nilssen, and A. Nysveen, "High-power generators for offshore wind turbines," *Energy Procedia*, vol. 35, pp. 52–61, 2013.

[12] R. S. Semken, M. Polikarpova, P. Röyttä, J. Alexandrova, J. Pyrhönen, J. Nerg, A. Mikkola, and J. Backman, "Direct-drive permanent magnet generators for high-power wind turbines: Benefits and limiting factors," *IET Renewable Power Generation*, vol. 6, no. 1, pp. 1–8, 2012.

[13] Y. Wang and N. Bianchi, "Modeling and Investigation of Self-Excited Reluctance Generators for Wind Applications," *IEEE Transactions on Industry Applications*, vol. 55, no. 6, pp. 5809–5817, 2019.

[14] A. Mohammadi, Y. Chulaee, A. M. Cramer, I. Boldea, and D. M. Ionel, "Axial Flux Permanent Magnet Vernier Machine with Single-wound Dual-stator and Spoke Permanent Magnet Rotor for Electric Vehicle In-wheel Traction," in *2023 IEEE Transportation Electrification Conference & Expo (ITEC)*, 2023, pp. 1–5.

[15] M. Lehr, D. Dietz, and A. Binder, "Electromagnetic design of a permanent magnet Flux-Switching-Machine as a direct-driven 3 MW wind power generator," in *2018 IEEE International Conference on Industrial Technology (ICIT)*. IEEE, 2018, pp. 383–388.

[16] C. J. J. Labuschagne and M. J. Kamper, "Design and Performance Evaluation of PM Vernier Generator Technology for a Small-Scale Uncontrolled Passive Wind Generator System," *IEEE Transactions on Industry Applications*, vol. 58, no. 4, pp. 4657–4667, 2022.

[17] T. Husain, I. Hasan, Y. Sozer, I. Husain, and E. Muljadi, "A Comprehensive Review of Permanent Magnet Transverse Flux Machines: Use in Direct-Drive Applications," *IEEE Industry Applications Magazine*, vol. 26, no. 6, pp. 87–98, 2020.

[18] Y. Chen, P. Pillay, and A. Khan, "PM wind generator topologies," *IEEE Transactions on Industry Applications*, vol. 41, no. 6, pp. 1619–1626, 2005.

[19] I. Boldea, L. N. Tutelea, I. Torac, and F. Marignetti, "10MW, 10rpm, 10Hz directly-driven cage rotor induction generator (CRIG): preliminary design with key FEM validations," in *2019 International Aegean Conference on Electrical Machines and Power Electronics (ACEMP) & 2019 International Conference on Optimization of Electrical and Electronic Equipment (OPTIM)*, 2019, pp. 65–70.

[20] I. Boldea, L. N. Tutelea, and I. Torac, "10MW, 10rpm, 15Hz directly-driven reluctance synchronous generator system: preliminary design with key FEM validations," in *2020 International Conference on Electrical Machines (ICEM)*, vol. 1, 2020, pp. 1835–1840.

[21] I. Boldea, I. Torac, and L. Tutelea, "ALA-Rotor RSG 10MW, 480RPM-Preliminary Design with 2D Key FEM Validations," in *2023 22nd International Symposium on Power Electronics (Ee)*, vol. 1, 2023, pp. 1–5.

[22] U. B. Akuru and M. J. Kamper, "Intriguing Behavioral Characteristics of Rare-Earth-Free Flux Switching Wind Generators at Small- and Large-Scale Power Levels," *IEEE Transactions on Industry Applications*, vol. 54, no. 6, pp. 5772–5782, 2018.

[23] W. Ullah, F. Khan, U. B. Akuru, S. Hussain, M. Yousuf, and S. Akbar, "A novel dual electrical and dual mechanical wound field flux switching generator for co-rotating and counter-rotating wind turbine applications," *IEEE Transactions on Industry Applications*, pp. 1–12, 2023.

[24] W. Ullah, F. Khan, U. B. Akuru, and M. Yousuf, "Magnetic Coupling Effect and Performance Analysis of Dual Rotor Permanent Magnet Flux Switching Generator for Counter Rotating Wind Power Generation," *IEEE Transactions on Energy Conversion*, vol. 38, no. 4, pp. 2895–2908, 2023.

[25] P. Han, M. G. Kesgin, D. M. Ionel, R. Gosalia, N. Shah, C. J. Flynn, C. S. Goli, S. Essakiappan, and M. Manjrekar, "Design optimization of a very high power density motor with a reluctance rotor and a modular stator having PMs and toroidal windings," in *2021 IEEE Energy Conversion Congress and Exposition (ECCE)*, 2021, pp. 4424–4430.

[26] O. A. Badewa, A. Mohammadi, D. D. Lewis, D. M. Ionel, S. Essakiappan, and M. Manjrekar, "Optimization of an Electric Vehicle Traction Motor with a PM Flux Intensifying Stator and a Reluctance Outer Rotor," in *2023 IEEE Transportation Electrification Conference & Expo (ITEC)*, 2023, pp. 1–6.

[27] G. Heins, D. M. Ionel, and M. Thiele, "Winding Factors and Magnetic Fields in Permanent-Magnet Brushless Machines With Concentrated Windings and Modular Stator Cores," *IEEE Transactions on Industry Applications*, vol. 51, no. 4, pp. 2924–2932, 2015.

[28] M. G. Kesgin, P. Han, D. Lawhorn, and D. M. Ionel, "Analysis of torque production in axial-flux vernier PM machines of the MAGNUS type," in *2021 IEEE International Electric Machines & Drives Conference (IEMDC)*. IEEE, 2021, pp. 1–5.

[29] R. Storn and K. Price, "Differential Evolution – A Simple and Efficient Heuristic for global Optimization over Continuous Spaces," in *Journal of Global Optimization*, vol. 11, 1997, pp. 341–359.

[30] M. Rosu, P. Zhou, D. Lin, D. M. Ionel, M. Popescu, F. Blaabjerg, V. Rallabandi, and D. Staton, *"Multiphysics Simulation by Design for Electrical Machines, Power Electronics and Drives"*. J. Wiley - IEEE Press, 2017.

[31] *Ansys® Electronics, Maxwell, version 23.1, 2023, ANSYS Inc.*

[32] Niron Magnetics, "Niron Magnetics: Magnets Rare Earth vs. Clean Earth," *Minneapolis, Minnesota, USA*, accessed March 2023. [Online]. Available: https://www.nironmagnetics.com/#OurTechnology

[33] L. Fingersh, M. Hand, and A. Laxson, "Wind turbine design cost and scaling model," National Renewable Energy Lab (NREL), Golden, CO, United States, Tech. Rep., 2006.

[34] N. Taran, D. M. Ionel, V. Rallabandi, G. Heins, and D. Patterson, "An Overview of Methods and a New Three-Dimensional FEA and Analytical Hybrid Technique for Calculating AC Winding Losses in PM Machines," *IEEE Transactions on Industry Applications*, vol. 57, no. 1, pp. 352–362, 2021.

Ali Mohammadi (Graduate Student Member, IEEE) received the B.Sc. and M.Sc. degrees from the Babol Noshirvani University of Technology, Babol, Iran, both in electrical engineering, in 2016 and 2020, respectively. He is currently working toward the Ph.D. degree with SPARK Laboratory, Department of Electrical and Computer Engineering, University of Kentucky, Lexington, KY, USA. He was the recipient of the Best Paper Award as first author at the 2022 IEEE International Conference on Renewable Energy Research and Applications (ICRERA), the Best Student Paper Award as first author at the 2023 IEEE Transportation Electrification Conference (ITEC), and the First Best Paper Award as a co-author at the 2023 IEEE International Conference on Renewable Energy Research and Applications (ICRERA) all on topics of specialty electric machines. His research focuses on renewable energies, electrification of transportation, advanced electromagnetic FEA, the design and optimization of electric machines, motor drives and power electronics.

Badewa Oluwaseun (Graduate Student Member, IEEE) received the B.Sc. degree from ATBU, Bauchi, Nigeria, and the M.Sc. degree from CAU, Kiel, Germany both in Electrical engineering. From 2016 to 2020, he worked as a Senior Electrical engineer with DORCL, Nigeria specialized in electrical design and detailed engineering, and commissioning for petrochemical complexes. He is currently working toward the Ph.D. degree with SPARK Laboratory, Department of Electrical and Computer Engineering, University of Kentucky, Lexington, KY, USA. He was the co-recipient of the Best Paper Award at the 2022 IEEE International Conference on Renewable Energy Research and Applications (ICRERA) with a paper on multi-MW direct-drive wind-turbine generators employing a flux intensifying PM stator and reluctance rotor novel topology. At UK, he has been working as a Research Assistant with research interests in electric machines and power electronic drives.

Yaser Chulaee (Graduate Student Member, IEEE) received the B.Sc. degree in electrical engineering from the Shahrood University of Technology, Shahrood, Iran, in 2016, and the M.Sc. degree in electrical engineering from the Ferdowsi University of Mashhad, Mashhad, Iran, in 2019. He is currently working toward the Ph.D. degree with SPARK Laboratory, Department of Electrical and Computer Engineering, University of Kentucky, Lexington, KY, USA. His research focuses on advanced electromagnetic FEA, the design and optimization of electric machines, and motor drive systems. He was the recipient of a best paper award as a co-author at the 2022 IEEE International Conference on Renewable Energy Research and Applications (ICRERA), a best paper award as a co-author at the 2023 IEEE Transportation Electrification Conference (ITEC 2023), and a prize paper by the Electric Machines Committee of the IEEE Industrial Applications Society for a paper presented at the 2022 Energy Conversion Conference and Exposition (ECCE 2022).

Donovin Lewis (Graduate Student Member, IEEE) received the B.Sc. degree in electrical engineering in 2021 from the University of Kentucky, Lexington, KY, USA, where he is working toward the Ph.D. degree with the SPARK Laboratory, Department of Electrical and Computer Engineering. He is also a remote research collaborator with Oak Ridge National Laboratory, and a summer visitor with the University of Oxford, Oxford, England. During his undergraduate studies, he was a William C. Parker Scholar, a NASA REU student and has been recognized by the UK Stanley and Karen Pigman COE with the 2023 Outstanding PhD Student Award. He was the Chief Electrical Engineer of the 2021 U.S. National Champion University of Kentucky Solar Car Team. His research interests include wireless charging of electric vehicles, electric motors, and renewable energy integration. He is a National Science Foundation (NSF) Graduate Research Fellow, was a University of Kentucky Otis A. Singletary Graduate Fellow, and a former recipient of the IEEE PES Plus Scholarship.

Somasundaram Essakiappan (Senior Member, IEEE) received the B.E. degree in Electrical and Electronics Engineering from the College of Engineering Guindy, in 2007, and the M.S. and Ph.D. degrees in Electrical Engineering from Texas A&M University, in 2010 and 2014, respectively. He has been an Adjunct Professor with the Department of Electrical and Computer Engineering, The University of North Carolina at Charlotte, since 2015, where he is responsible for courses in power and leading sponsored research projects. Previously, he was a Research and Development Engineering Manager with QM Power Inc., responsible for leading programs on new motor architectures and motor drive development projects, from 2021 to 2023. Prior to that, he was a Teaching Professor and the Manager of the Flexible Energy Laboratories, Energy Production and Infrastructure Center, The University of North Carolina at Charlotte, from 2016 to 2021, where he developed and managed a high-power research and industrial testing laboratory for power electronic systems. He has published more than 50 research articles in various disciplines of power engineering. He is an inventor of two awarded U.S. patents and multiple pending patent applications. His research interests include power electronics for distributed energy integration, power quality and resiliency, and motors and drives. He is an active volunteer in professional societies and serves as a member of the Power Electronics Society Magazine Advisory Board and a reviewer for major journals and conferences. In the past, he has served as the Chair of the Young Professionals of IEEE Power Electronics Society, the Technical Program Chair for the 9th and 12th editions of the International Symposium on Power Electronics for Distributed Generation Systems (IEEE-PEDG), and the Publications Chair for the 11th Workshop on Wide Bandgap Power Devices and Applications (IEEE-WiPDA).

Madhav D. Manjrekar (Senior Member, IEEE) was born in 1972. He received the B.E. degree from the Government College of Engineering, University of Pune, India, in 1993, the M.Tech. degree from the Center for Electronic Design and Technology, Indian Institute of Science, India, in 1995, the M.S. degree from Montana State University, Bozeman, in 1997, the Ph.D. degree in electrical engineering from the University of Wisconsin, Madison, in 1999, and joined the University of North Carolina – Charlotte as an Associate Professor of Electrical & Computer Engineering in 2012. Prior to joining academia, he worked as the Vice President of Global Research and Innovation at Vestas, and previously has held various leadership and management positions at Siemens, Eaton and ABB. Dr. Manjrekar holds over 10 US and international patents, has published over 125 journal and conference papers, and has received multiple IEEE prize paper awards. He has advised over 30 PhD and MS students and currently serves as an Assistant Director and Chief Research Officer of the Energy Production and Infrastructure Center (EPIC) at the university.

Dan M. Ionel (Fellow, IEEE) received the M.Eng. and Ph.D. degrees in electrical engineering from the Polytechnic University of Bucharest, Bucharest, Romania. His doctoral program included a Leverhulme Visiting Fellowship with the University of Bath, Bath, U.K. He was a Post-doctoral Researcher with the SPEED Laboratory, University of Glasgow, Glasgow, U.K.

He is currently a Professor of electrical engineering and the L. Stanley Pigman Chair in Power with the University of Kentucky, Lexington, KY, USA, where he is also the Director of the Power and Energy Institute of Kentucky and of the SPARK Laboratory. Previously, he worked in industry, most recently as Chief Engineer with Regal Beloit Corporation, Grafton, WI, USA, and before that as Chief Scientist with Vestas Wind Turbines. He was also a Visiting Professor and a Research Professor with the University of Wisconsin and Marquette University, Milwaukee, WI. He has contributed to technology developments with long lasting industrial impact, designed electric machines and drives with ratings between 0.002 and 1,000hp, holds more than 40 patents, and has authored or coauthored two books and more than 300 technical papers, including IEEE award winners.

He was a recipient of the Cyril G. Veinott Award from the IEEE Power and Energy Society (PES). He was the Inaugural Chair of the IEEE Industry Applications Society Renewable and Sustainable Energy Conversion Systems Committee, and an Editor of IEEE Transactions on Sustainable Energy. He was the Chair of the IEEE PES Electric Motor Subcommittee, the General Chair of the IEEE 2017 Anniversary Edition of the International Conference on Electrical Machines and Drives (IEMDC), and Chair of the IEEE IEMDC Steering Committee.